Original Article

Dynamic characteristics assessment of reactor vessel internals with fluid-structure interaction

Sang Yun Je [a], Yoon-Suk Chang [a, *], Sung-Sik Kang [b]

[a] Department of Nuclear Engineering, Kyung Hee University, 1732 Deogyeong-daero, Giheung-gu, Yongin-si, Gyeonggi-do 17104, Republic of Korea
[b] Korea Institute of Nuclear Safety, 34 Gwahak-ro, Yuseong-gu, Daejeon-si, 34142, Republic of Korea

ABSTRACT

Improvement of numerical analysis methods has been required to solve complicated phenomena that occur in nuclear facilities. Particularly, fluid-structure interaction (FSI) behavior should be resolved for accurate design and evaluation of complex reactor vessel internals (RVIs) submerged in coolant. In this study, the FSI effect on dynamic characteristics of RVIs in a typical 1,000 MWe nuclear power plant was investigated. Modal analyses of an integrated assembly were conducted by employing the fluid-structure (F-S) model as well as the traditional added-mass model. Subsequently, structural analyses were carried out using design response spectra combined with modal analysis data. Analysis results from the F-S model led to reductions of both frequency and Tresca stress compared to those values obtained using the added-mass model. Validation of the analysis method with the FSI model was also performed, from which the interface between the upper guide structure plate and the core shroud assembly lug was defined as the critical location of the typical RVIs, while all the relevant stress intensities satisfied the acceptance criteria.

© 2017 Korean Nuclear Society, Published by Elsevier Korea LLC. This is an open access article under the CC BY-NC-ND license (http://creativecommons.org/licenses/by-nc-nd/4.0/).

1. Introduction

Reactor vessel internals (RVIs) perform safety-related functions such as holding up the nuclear fuel assembly, provide coolant passage through the reactor core, and support the control element drive mechanism. In the case of the functional loss of RVIs, the nuclear fuel assembly will be damaged and subsequent failure of the reactor pressure vessel (RPV) due to impact of fallen parts may lead to severe accidents. Hence, during the past several decades, diverse analyses and experiments have been carried on the internals in order to resolve relevant safety concerns. However, from the point of view of design and evaluation, there is still room for improvement of analysis methods related to complicated physical phenomena and insufficient computational accuracy. For instance, realistic dynamic characteristics and behaviors of complex RVIs have not been explicitly taken into account for practical applications.

Many recent studies have focused on the structural integrity assessment of RVIs and other major components. Jhung and Ryu [1] performed response spectra and time history analyses of a simple mechanical component against earthquakes, and compared their results. Several base excitation types were considered and special attention was recommended as a basis for further dynamic analysis. Park et al. [2] examined the modal characteristics of RVIs based on scale-similarity analysis with fluid-structure interaction (FSI). It was observed that the added-mass (A-M) model for submerged structures is considerably dependent on mode shapes and natural frequencies. Sigrist et al. [3] also conducted comparative dynamic analyses with FSI modeling for pressure vessel and internals in a nuclear reactor. They proved that the coupling effect is significant, whereas the effect of added-stiffness on global behavior is negligible. Choi et al. [4] identified dynamic characteristics of a scale-down System-integrated Modular Advanced ReacTor (SMART) by FSI modeling. They showed that the overall natural frequencies in water decrease dramatically compared with those obtained from totally assembled reactor internals in air. In addition, dynamic characteristics were investigated by considering holes and sloshing at free vibration conditions [5–8]. Seismic responses were analyzed for butterfly valves, reactor coolant pump, and reactor internals [9–12], and the FSI effects were evaluated: not only thermal fatigue, but also comprehensive vibration assessment [13,14]. However, most of these numerical studies did not incorporate actual complex structural geometry or realistic analysis conditions, which might contribute to the lack of accuracy.

---

* Corresponding author.
E-mail address: yschang@khu.ac.kr (Y.-S. Chang).

In this paper, we examined the effects of the FSI on the dynamic characteristics of the internals in an integrated assembly in a typical 1,000 MWe nuclear power plant. At first, modal analyses were performed using both traditional A-M and alternative FSI models to determine individual mode shapes and frequencies. Subsequently, structural analyses were carried out using design response spectra combined with the modal analyses data. Finally, to ensure structural integrity of the internals after validating the analysis method with the FSI, differences of the two sets of analyses were investigated in detail and resulting stress intensities were compared with the corresponding limit values based on ASME (American Society of Mechanical Engineers) B&PV (Boiler and Pressure Vessel) Code Section III, Subsection NG [15].

2. Analysis conditions and method

2.1. Brief description of RVIs

The RVIs dealt with in this study are classified into two major parts of core support barrel (CSB) assembly and upper guide structure (UGS) assembly. The CSB assembly includes the CSB itself, the lower support structure (LSS), the in-core instrumentation nozzle assembly, and the core shroud assembly (CSA). The CSB is a circular cylinder supported from a ledge on the RPV by a ring flange; the CSB carries the entire weight of the core. There are six equally spaced snubbers at the bottom of the CSB that prevent torsional motion of the internals. The LSS transmits the weight of the core to the CSB by means of a grid beam structure. The CSA surrounds the core and minimizes the amount of bypass flow. By contrast, the UGS assembly is located above the reactor core within the CSB. Its main functions are to align and support the fuel assemblies, maintain the control element assembly shroud spacing, prevent movement of the fuel assemblies in case of severe accident conditions, and protect the control rods from cross-flow effect.

2.2. Modeling details

In order to investigate the dynamic characteristics of the RVIs, three-dimensional finite element (FE) models were developed using a general purpose program (ANSYS Workbench version 17.2; ANSYS Inc., Canonsburg, PA, USA). Fig. 1 depicts a typical assembled model consist of the CSA, UGS, CSB, and LSS with encompassing fluid, as well as the RPV and four support columns. Since the amount of cooling water moving to the upper head of the RPV through the UGS was less than 0.1% of the total water quantity, it was not modeled due to effective computational time, as well as negligible flow effect [16]. Each subcomponent with coolant, and the RPV with support columns, were modeled using solid structure elements (element type Solid 185) and fluid elements (element type Fluid 221) in the ANSYS library (ANSYS Inc.), respectively.

Boundary conditions were set by considering the states of the subcomponent assembly according to the design documents, as shown in Fig. 2. Especially, the upper flange of the CSB was assembled with a reactor upper head by alignment keys; these keys were connected to top of the UGS by a hold down ring. Thus, the degrees of freedom (DOFs) of the upper CSB were fixed along the vertical and circumferential directions. UGS fuel alignment plate and CSA guide lug were coupled by insert pins so that the jointing parts were fully fixed. Additionally, since the CSB snubber lugs were tied to the vessel core stabilizing lugs and the cold leg nozzles were welded to the supports, the DOFs of the lower CSB were fixed along the circumferential direction and the bottoms of the support column were fully fixed. Materials of the RPV and RVIs considered in this study are SA508 carbon steel and TP 304 stainless steel, respectively; their properties at operating temperature with damping ratios are summarized in Table 1.

2.3. FSI analysis methods

There are two well-known methods to evaluate the interaction between a structure and an acoustic fluid: one is pressure-based formulation and the other is displacement-based formulation. Although the latter formulation is easier to implement due to the construction of symmetric mass and stiffness matrices, it suffers from spurious resonances. While the former formulation generates nonsymmetric matrices and unnecessary eigenmodes of the fluid, it has the advantage of fewer unknowns [17]. In this research, both methods were examined for comparison.

At first, the following dynamics equation was employed to consider the fluid as an A-M [2,18]:

$$[M_s]\{\ddot{u}\} + [C_s]\{\dot{u}\} + [K_s]\{u\} = \{f_e\} + \left\{f_f\right\} \tag{1}$$

where $[M_s]$, $[C_s]$, and $[K_s]$ denote the mass, damping, and stiffness matrices, respectively, and $\{\ddot{u}\}$, $\{\dot{u}\}$, and $\{\ddot{u}\}$ are the acceleration, velocity, and displacement vectors for the structure. In Eq. (1), the total load applied to the structure is given by sum of the external force vector, $\{f_e\}$, and the hydrodynamic force vector, $\{f_f\}$, at the fluid-structure (F-S) interface. The hydrodynamic force can be obtained from the integral of the fluid pressure vector $\{p\}$ with respect to the infinitesimal interface area dS, as in Eq. (2). Here, $\{Np\}$ is the approximating shape function for the spatial variation of the pressure, $\{n\}$ is the unit vector normal to the fluid-structure interface, and $[M_a]$ is the A-M matrix:

$$\left\{f_f\right\} = \int_S \{N_p\}^T \{n\}\{p\}dS = -[M_a]\{\ddot{u}\} \tag{2}$$

Substituting Eq. (2) into Eq. (1) yields:

$$([M_s] + [M_a])\{\ddot{u}\} + [C_s]\{\dot{u}\} + [K_s]\{u\} = \{f_e\} \tag{3}$$

Thus, the dynamic characteristic equation including the A-M causes a reduction of the frequencies.

Alternatively, the FSI can be evaluated by considering the coupling structural and fluid behaviors. The well-known structural dynamics equation was modified to consider the fluid pressure transferred to the structure:

$$[M_s]\{\ddot{u}\} + [C_s]\{\dot{u}\} + [K_s]\{u\} - [R_{int}]\{p\} = \{f_e\} \tag{4}$$

where $[R_{int}]$ is the stiffness matrix of the fluid interacting boundary. By contrast, fluid momentum and continuity equations were simplified using the acoustic wave equation to take into account the coupling mass matrix at the interface, as in [4,18]:

$$\left[M_f\right]\{\ddot{p}\} + \left[C_f\right]\{\dot{p}\} + \left[K_f\right]\{p\} + \rho[R_{int}]^T\{\ddot{u}\} = \{0\} \tag{5}$$

where $[M_f]$, $[C_f]$, and $[K_f]$ denote the mass, damping, and stiffness matrices of the fluid, respectively, and ρ is the fluid density, so that $\rho[R_{int}]^T$ represents the coupling mass matrix at the F-S interface. Consequently, we simultaneously solved the following discretized matrices, for which the aforementioned fluid elements (element type Fluid 221 in ANSYS library) were adopted:

$$\begin{bmatrix} [M_s] & 0 \\ \rho[R_{int}]^T & [M_f] \end{bmatrix} \left\{ \begin{matrix} \{\ddot{u}\} \\ \{\ddot{p}\} \end{matrix} \right\} + \begin{bmatrix} [C_s] & 0 \\ 0 & [C_f] \end{bmatrix} \left\{ \begin{matrix} \{\dot{u}\} \\ \{\dot{p}\} \end{matrix} \right\}$$
$$+ \begin{bmatrix} [K_s] & -[R_{int}] \\ 0 & [K_f] \end{bmatrix} \left\{ \begin{matrix} \{u\} \\ \{p\} \end{matrix} \right\} = \left\{ \begin{matrix} f_e \\ 0 \end{matrix} \right\}$$

2.4. Acceptance criteria

The ASME code [15] categorizes stress components into general primary membrane stress intensity, P_m, local membrane stress
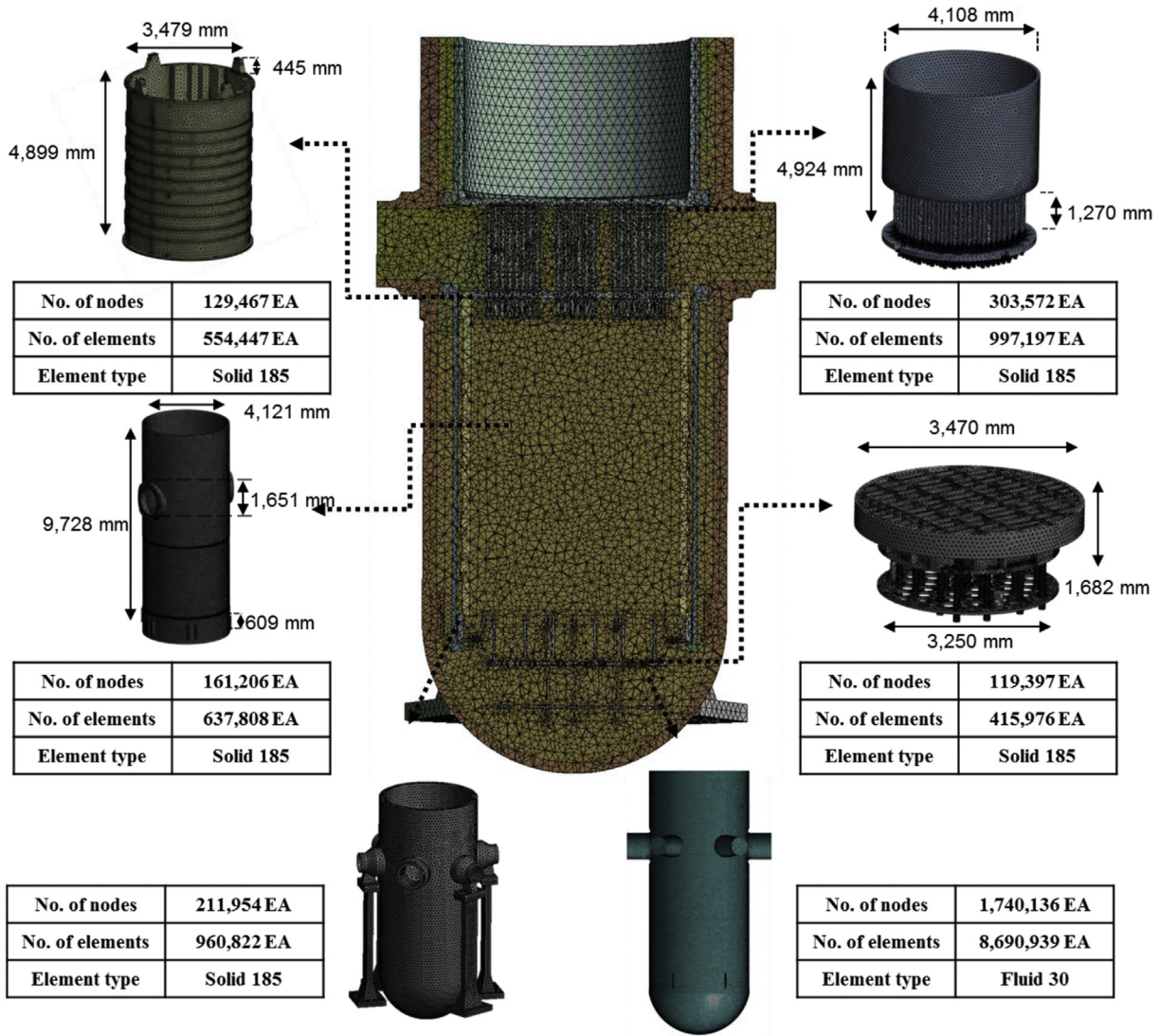
Fig. 1. Typical assembled finite element (FE) model.

intensity, P_L, and primary bending stress intensity, P_b. It also specifies acceptance criteria that should be satisfied for each stress intensity and combination of them. With regard to RVIs made of stainless steel, the following conditions should be met:

$$\min[2.4S_m, \ 0.7S_u] \geq P_m \tag{7}$$

$$1.5 \min [2.4S_m, 0.7S_u] \geq P_m + P_b \tag{8}$$

where S_m is the allowable design stress intensity and S_u is the tensile strength as defined in the code.

In general, using the stress analysis data, the membrane and bending stress intensities can be determined by the following equations:

$$P_m = \frac{1}{t} \int_{-t/2}^{t/2} P_i dx_s \tag{9}$$

$$P_b = \frac{-6}{t^2} \int_{-t/2}^{t/2} P_i x_s dx_s \tag{10}$$

where t is the thickness, P_i is the i stress component along any path produced by the design loads, and x_s is the coordinate along the path. The provision on the limit analysis with collapse load was not considered in this study because sufficiently lower values of stress components were determined in the FE analyses.

3. FE analyses

3.1. Validation of analysis method with FSI

To check the validity of the present analysis method with FSI, a fluid-filled co-axial cylindrical shell was selected from a recent study [19]. The height, mean radius of inner cylinder, and mean radius of the outer cylinder were 972 mm, 203 mm, and 245 mm, respectively. A three-dimensional FE mesh was generated as shown in Fig. 3, and material properties such as structural density of 2,700 kg/m^3 and water density of 1,000 kg/m^3 were taken from the reference. Fig. 4 compares benchmarking analysis results for the co-
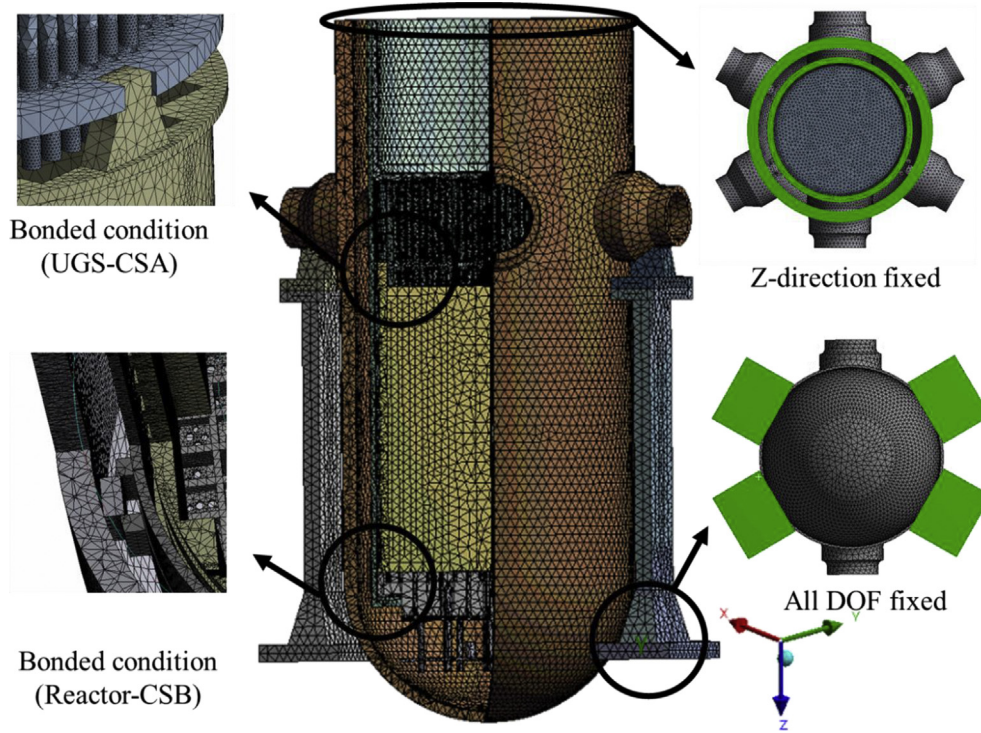
Fig. 2. Boundary conditions. CSA, core shroud assembly; CSB, core support barrel; DOF, degrees of freedom; UGS, upper guide structure.

Table 1
Material properties at operating temperature (290°C).

Material		Young's modulus(GPa)	Poisson's ratio	Density(kg/m³)	Damping ratio
RPV	SA508 Gr.3 Cl.1	200	0.29	8,000	0.03
RVI	SA240 TP 304	176	0.31	7,750	0.05

axial cylindrical shell. Frequencies calculated by the F-S interaction model based on Eq. (6) agreed with reference analysis data to within 5%, in spite of the different meshes and analysis codes, while the A-M model based on Eq. (3) overpredicted the corresponding frequencies.

3.2. Modal analysis

Modal analysis is necessary to predict the dynamic characteristics of the components, such as the mode shapes and the natural frequencies, when it is not possible to perform modal test for large-sized real geometry. The FE model shown in Fig. 1 was optimized through preliminary analyses for both the assembly as well as each subcomponent with RPV and fluid. Structural connections like welds and bolting locations were treated by merging nodes.

For comparison, the coolant was modeled as either an equivalent A-M or as the fluid itself. In the case of the A-M model, the displacement-based formulation was adopted and its equivalent values were calculated according to the ASME code, as follows:

$$\rho \pi R_1^2 b \left[\frac{1 + \left(R_{1/R_2}\right)^2}{1 - \left(R_{1/R_2}\right)^2} \right] \text{ for inner cylinder} \tag{11}$$

$$\rho \pi R_2^2 b \left[\frac{1 + \left(R_{1/R_2}\right)^2}{1 - \left(R_{1/R_2}\right)^2} \right] \text{ for outer cyclinder} \tag{12}$$

where ρ is the fluid density, R_1 is the radius of inner cylinder, R_2 is the radius of outer cylinder, and b is the length of the section. By contrast, in the case of the F-S model, the pressure-based formulation was adopted by setting the interfaces before the analysis.

3.3. Response spectrum analysis

Structural analyses under earthquake loads can be carried out by either the response spectrum method or time history method; the latter method usually evaluates the structural behavior as a function of time and in terms of acceleration. This method provides accurate results but is highly time-consuming and requires complicated procedures with detailed input data for the analysis. By contrast, while the former method only approximately estimates the structural behavior, it has been widely adopted for component design due to its relatively simple and reasonably accurate features. In this study, structural analyses were conducted using the response spectrum method. By designating specific vectors with the modal analysis data at all significant modes, as load sets, the structural responses, R_i, such as stress, strain, displacement, moment, etc. were calculated as follows:

$$R_i = \gamma_i S_i \{\varphi\}_i \tag{13}$$

where γ_i, S_i, and $\{\varphi\}_i$ are the participation factor, response spectrum value, and eigenvector representing the mode shape at the ith mode, respectively.

Moreover, there are two typical ways of combining the structural responses such as the square root of the sum of squares and the complete quadratic combination (CQC) techniques [20]. In the
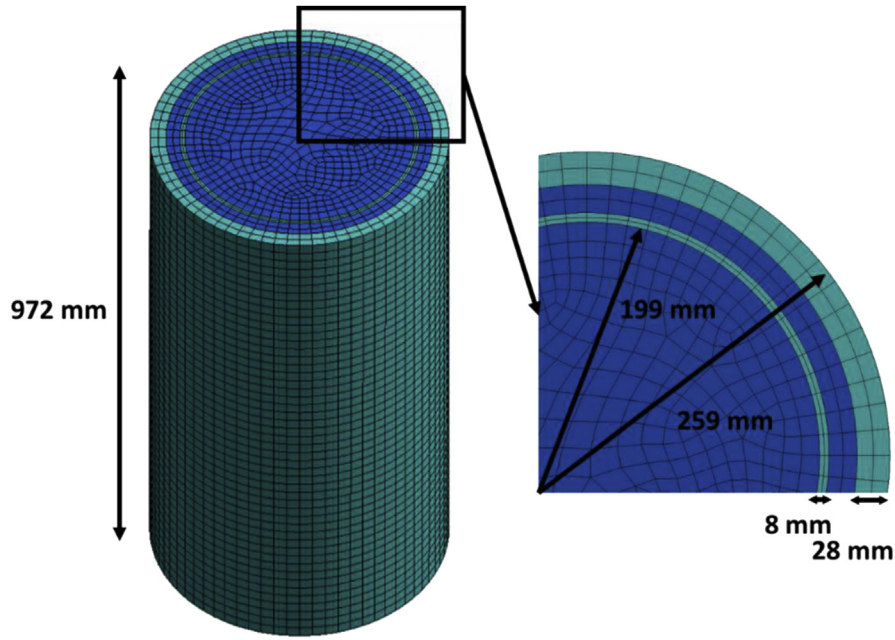
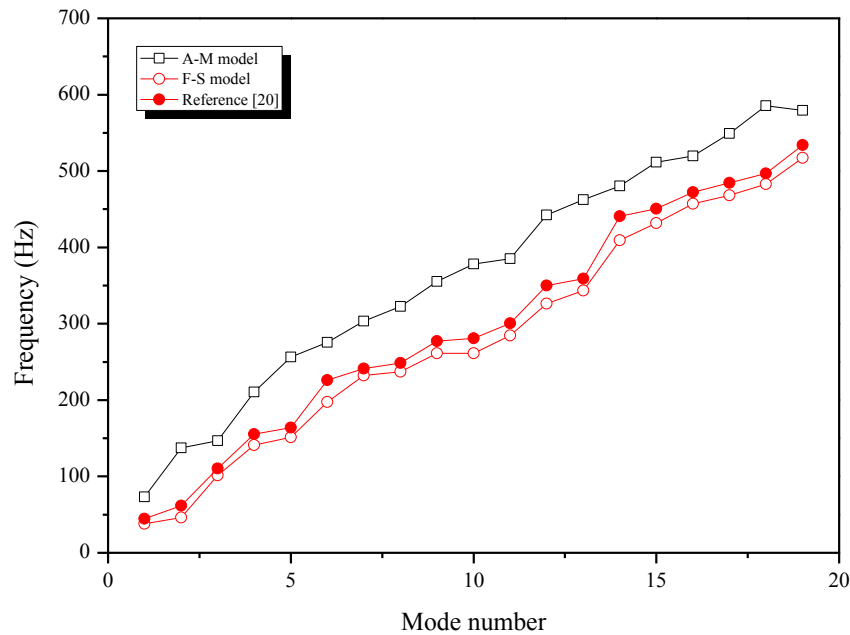Fig. 3. Geometry and FE mesh of a fluid-filled co-axial cylindrical shell.

Fig. 4. Comparison of benchmarking analysis results of the co-axial cylindrical shell. A-M, added-mass; F-S, fluid-structure.

square root of the sum of squares technique, the total response of interests, R, is obtained by combining the peak modal responses as in:

$$R = \pm \left[\sum_{k=1}^{n} R_k{}^2 \right]^{\frac{1}{2}} \quad (14)$$

where R_k is the peak response of interest due to the kth mode and n is the number of significant modes. This technique provides relatively conservative results but often underestimates the combined response values in the case of closely spaced modes. Meanwhile,

the CQC technique combines responses based on cross-modal coefficients that reflect the correlation between modes, as well as the modal frequencies and damping ratios of the components. The total response of interests obtained using this technique can be written as:

$$R = \left[\sum_{i=1}^{N} \sum_{j=1}^{N} k \varepsilon_{ij} R_i R_j \right]^{\frac{1}{2}} \quad (15)$$

where k is 1 when $i = j$ or 2 when $i \neq j$. R_i and R_j represent the responses at the ith and jth modes. ε_{ij} designates the cross-modal

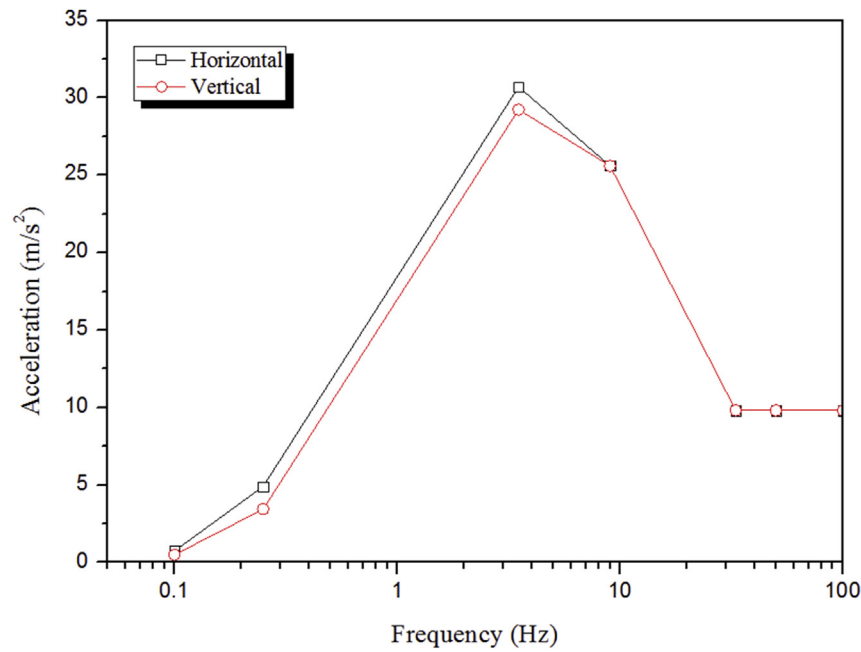Fig. 5. Design response spectra with 5% damping [21, 22].

(A)Mode #6 (32.35 Hz)   (B)Mode #7 (33.45 Hz)   (C)Mode #8 (38.50 Hz)

Fig. 6. Typical mode shapes of reactor vessel internals (RVIs) at the maximum effective mass condition along x-direction, y-direction, and z-direction [added-mass (A-M) model].

(A)Mode #11 (27.32Hz)   (B)Mode #12 (28.10 Hz)   (C)Mode #21 (41.31 Hz)
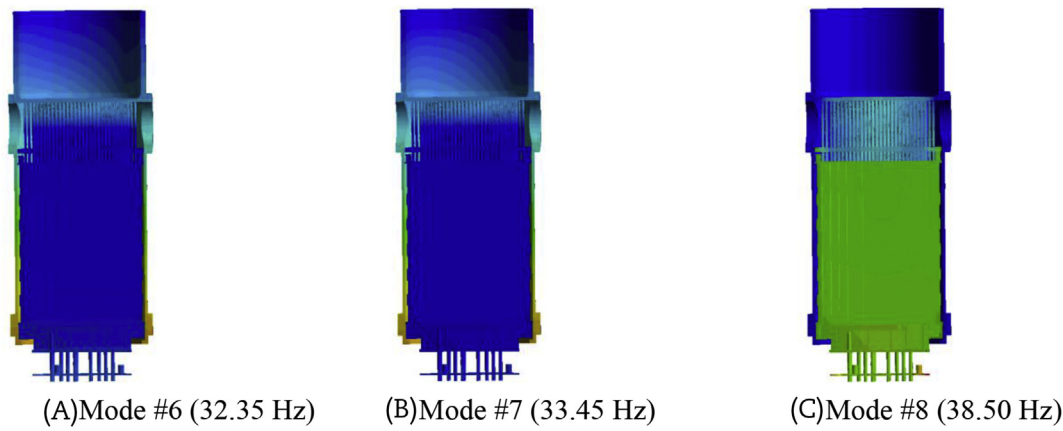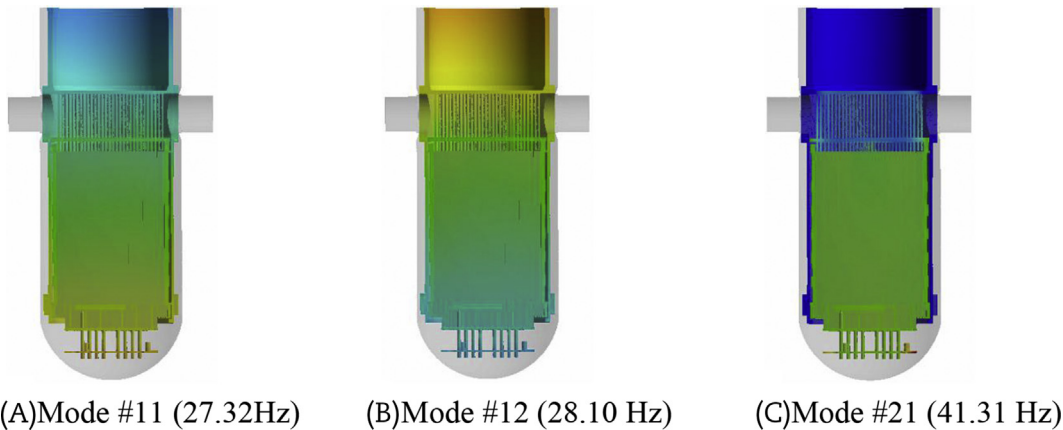
Fig. 7. Typical mode shapes of reactor vessel internals (RVIs) at the maximum effective mass condition along x-direction, y-direction, and z-direction [fluid-structure (F-S) model].

Table 2
Summary of representative modal analysis results.

Mode number	Frequency(Hz)		Effective mass					
			x-direction		y-direction		z-direction	
	A-M	F-S	A-M	F-S	A-M	F-S	A-M	F-S
1	8.03	3.33	25,115	1,287	77,403	7,755	$<10^{-2}$	$<10^{-2}$
2	8.10	3.35	77,523	7,708	25,152	1,255	$<10^{-2}$	$<10^{-2}$
3	9.36	9.91	$<10^{-2}$	$<10^{-2}$	$<10^{-2}$	$<10^{-2}$	$<10^{-2}$	$<10^{-2}$
4	22.84	16.68	7,343	$<10^{-2}$	22,498	1	$<10^{-2}$	2
5	23.02	17.14	23,891	$<10^{-2}$	7,811	2	$<10^{-2}$	$<10^{-2}$
6	32.35	17.76	179,280	36	60,011	2,094	$<10^{-2}$	$<10^{-2}$
7	33.45	17.89	62,279	2,732	186,073	147	$<10^{-2}$	$<10^{-2}$
8	38.50	20.00	$<10^{-2}$	64	$<10^{-2}$	154	197	$<10^{-2}$
9	46.89	22.57	$<10^{-2}$	$<10^{-2}$	2	$<10^{-2}$	$<10^{-2}$	165
10	48.26	22.95	4,713	109	2,093	39	$<10^{-2}$	$<10^{-2}$
11	48.71	27.32	44	188,188	31	62,719	$<10^{-2}$	$<10^{-2}$
12	49.05	28.10	4,717	64,225	12,777	192,862	$<10^{-2}$	$<10^{-2}$
13	49.59	33.28	$<10^{-2}$	$<10^{-2}$	$<10^{-2}$	$<10^{-2}$	25	3,719
14	50.52	33.69	$<10^{-2}$	$<10^{-2}$	$<10^{-2}$	$<10^{-2}$	$<10^{-2}$	2
15	55.32	33.71	$<10^{-2}$	$<10^{-2}$	$<10^{-2}$	$<10^{-2}$	$<10^{-2}$	7
16	55.46	34.15	1	225	4	77	$<10^{-2}$	$<10^{-2}$
17	58.13	37.09	$<10^{-2}$	11	$<10^{-2}$	33	$<10^{-2}$	$<10^{-2}$
18	58.72	39.23	$<10^{-2}$	$<10^{-2}$	$<10^{-2}$	$<10^{-2}$	$<10^{-2}$	738
19	59.78	40.15	3	1	$<10^{-2}$	$<10^{-2}$	$<10^{-2}$	2
20	60.13	40.18	35	1	6	2	$<10^{-2}$	12

A-M, added-mass; F-S, fluid-structure.
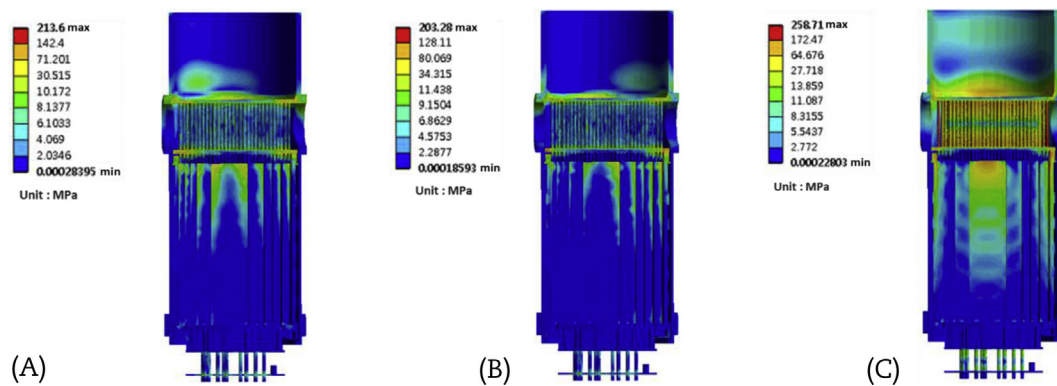
Fig. 8. Directional stress distributions calculated by added-mass (A-M) model. (A) x-direction. (B) y-direction. (C) z-direction.
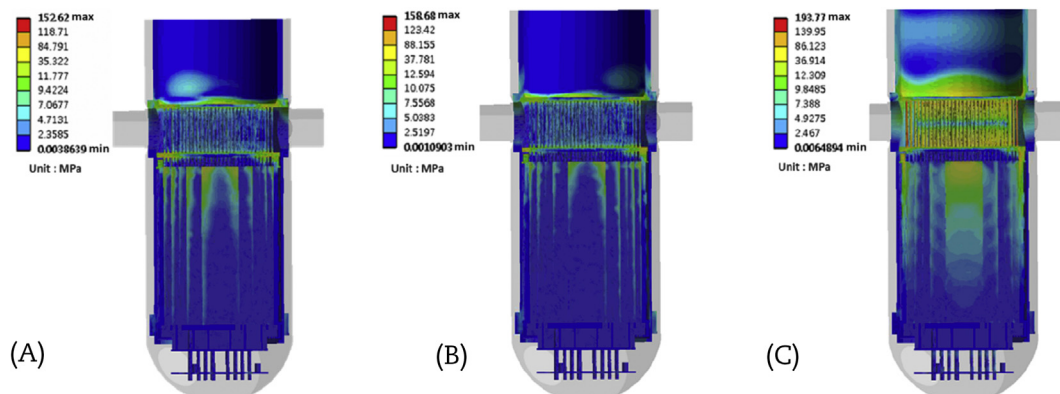
Fig. 9. Directional stress distributions calculated by fluid-structure (F-S) model. (A) x-direction. (B) y-direction. (C) z-direction.

coefficient presenting the correlation between the ith and jth modes, which can be expressed as:

$$\varepsilon_{ij} = \frac{8(\xi_i\xi_j)^{\frac{1}{2}}(\xi_i + r\xi_j)^{3/2}}{(1-r^2)^2 + 4\xi_i\xi_j r(1+r^2) + 4(\xi_i^2 + \xi_j^2)r^2} \tag{16}$$

where r and ξ are the ratio of frequencies and the modal damping, respectively.

In this study, design response spectra with 5% damping, as depicted in Fig. 5 [21,22], were applied at the bottoms of the RPV support columns. Particularly, the vertical response spectrum along the z-direction as well as the horizontal response spectrum along the x-direction and y-direction was considered. In addition, the CQC technique was employed to combine structural responses.
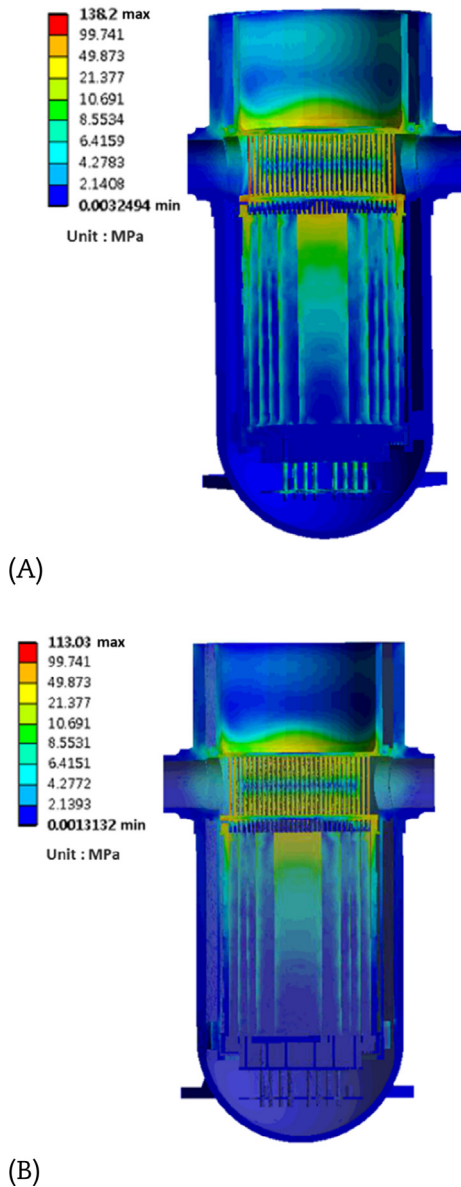

(A)

(B)

Fig. 10. Tresca stress distributions. (A) added-mass (A-M) model. (B) fluid-structure (F-S) model.

4. Results and discussion

Figs. 6 and 7 depict typical mode shapes of the assembled RVIs, determined by A-M and F-S models under the maximum effective mass condition along each direction. In these figures, the RPV and support columns were intentionally eliminated to clearly show the modal analysis results. When the structure was analyzed when submerged in coolant, resultant frequencies decreased by 38.67%, on average, compared to those obtained from the traditional A-M model. For instance, the first modal frequency of the RVIs was calculated at 8.03 Hz using the A-M model and at 3.33 Hz using the F-S model. The difference was caused by the fluid induced supplementary DOFs. Table 2 summarizes the representative modal analysis results obtained from the two models; these values were extracted until a 70% sum of effective mass ratios, approximately based on the A-M model.

The trend of the subsequent response spectrum analysis results was also similar to that of the modal analysis results. Figs. 8 and 9 show the directional stress distributions, in which the z-directional values were highest and the mean difference of the z-directional stresses between the two models was 25.10%. Fig. 10 compares snapshots of the resulting Tresca stress distributions. The maximum Tresca stress value obtained from the A-M model was higher than that obtained from the F-S model; the difference between the two values was 18.21%.

Fig. 11 shows the stress classification lines (SCLs) that were set based on the four high stress points. In detail, three SCLs were defined near the maximum stress point for each subcomponent. For instance, SCLs 1–3 were determined because the stress value was high between the UGS plate and the CSA lug, as shown in Fig. 11A. For the total of 12 SCLs, satisfaction of the acceptance criteria in Eqs. (7) and (8) was assessed by using the two models. According to the ASME code, the S_m of TP 304 stainless steel at operating temperature was found to be 180 MPa [15]; P_m and P_b were calculated using Eqs. (9) and (10), respectively. As summarized in Table 3, SCL 2 was defined as the critical path; the F-S model can provide lower values of P_m and P_b than those provided by the A-M model. However, in relation to the dynamic behavior, all assessment results satisfied the requirements of stress intensity.

As described previously, when the F-S model was adopted for dynamic characteristics assessment, due to the presence of coolant, the calculated frequencies and stress components of the RVIs were lower than those determined using the A-M model. To make sense of these results, directional effective masses were examined in detail. As compared in Fig. 12, most of the effective masses determined by the A-M model were driven into the initial 10 mode numbers, while those of the F-S model were spread over 30 mode numbers. Also, as presented in Table 2 and Fig. 5, input accelerations, varying with the frequencies, dropped from 3.5 Hz to 33 Hz with the increase of the mode number. Therefore, it seems that the early concentrated effective masses in the conventional A-M model led to conservative stress values compared to those values of the more realistic F-S model.

5. Conclusion

In this study, the effects of the FSI on the dynamic characteristics and behaviors of the internals in a typical 1,000 MWe nuclear power plant were examined and the following key findings were derived. (1) When the coolant was realistically modeled by fluid elements for the modal analysis of RVIs, resultant frequencies
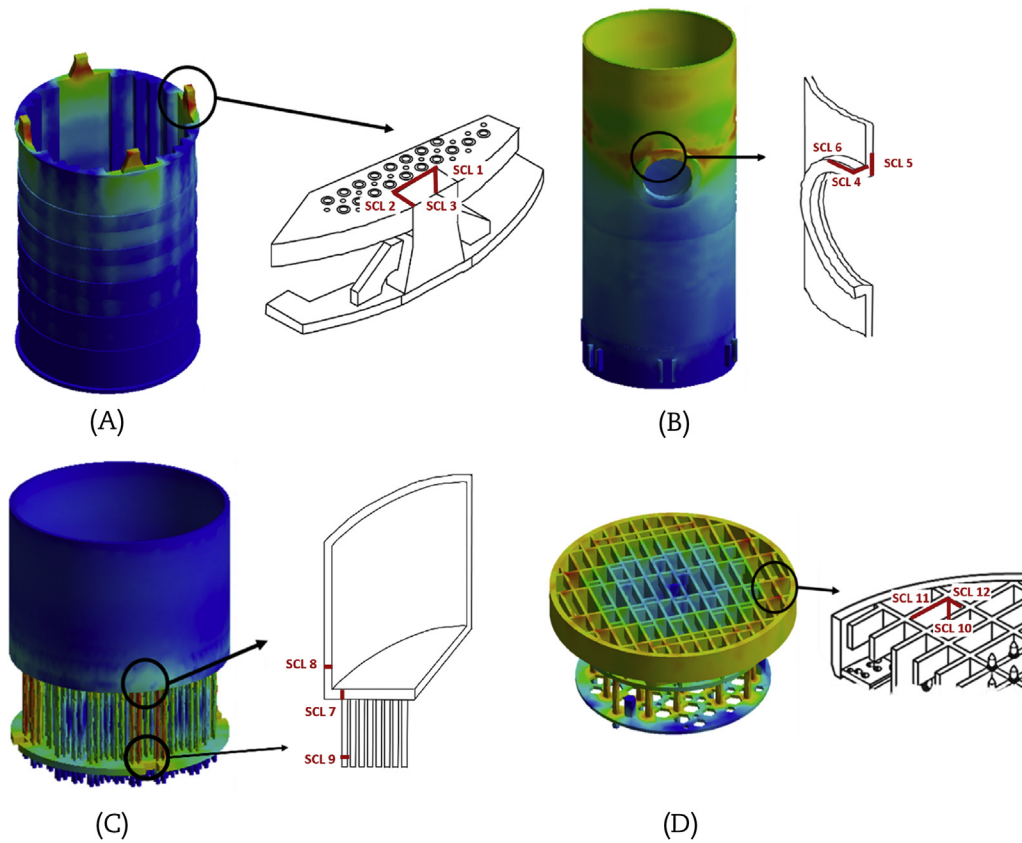
Fig. 11. Stress classification lines at each subcomponent. (A) core shroud assembly (CSA). (B) core support barrel (CSB). (C) upper guide structure (UGS). (D) lower support structure (LSS).

decreased by 39%, approximately, compared to those determined by the traditional A-M model. (2) Subsequent response spectrum analysis results showed that the maximum Tresca stresses dropped more than 18% when the alternative F-S model was employed. (3)

The interface between the UGS plate and the CSA lug was the critical location of the present RVIs. However, all the relevant general primary membrane stress intensities and local membrane stress intensities satisfied the corresponding acceptance criteria.

Table 3
Membrane and bending stress intensities of reactor vessel internals.

Location		P_m (MPa)			P_b (MPa)			$\frac{\min[2.4S_m,0.7S_u]}{P_m}$		$\frac{1.5\min[2.4S_m,0.7S_u]}{P_m+P_b}$	
		A-M	F-S	Difference (%)	A-M	F-S	Difference (%)	A-M	F-S	A-M	F-S
CSA	SCL 1	99.29	74.99	24.47	26.90	19.20	28.62	4.34	5.74	5.16	6.92
	SCL 2	114.50	89.24	22.06	2.86	2.05	28.32	3.76	4.82	5.55	7.14
	SCL 3	123.68	94.80	23.35	24.68	17.22	30.22	3.48	4.54	4.39	5.82
CSB	SCL 4	22.80	16.00	29.82	0.74	0.54	27.02	18.90	26.93	27.69	39.41
	SCL 5	4.40	4.01	8.86	0.24	0.09	62.5	97.95	107.48	140.51	159.02
	SCL 6	22.36	16.26	27.28	1.19	0.27	77.31	19.27	26.50	27.68	39.44
UGS	SCL 7	7.09	5.52	22.14	0.52	0.50	3.84	60.78	78.07	85.67	108.30
	SCL 8	9.53	6.59	30.84	0.37	0.36	2.70	45.22	65.40	65.85	93.81
	SCL 9	53.55	44.64	16.63	17.98	0.04	99.77	8.04	9.65	9.11	14.59
LSS	SCL 10	4.31	3.82	11.36	1.86	1.56	16.12	100.00	112.82	105.67	121.18
	SCL 11	7.31	6.56	10.25	5.31	4.98	6.21	58.96	65.70	51.66	56.49
	SCL 12	7.59	6.63	12.64	4.85	4.35	10.30	56.78	65.01	52.41	59.38

A-M, added-mass; CSA, core shroud assembly; CSB, core support barrel; F-S, fluid-structure; LSS, lower support structure; SCL, stress classification line; UGS, upper guide structure.
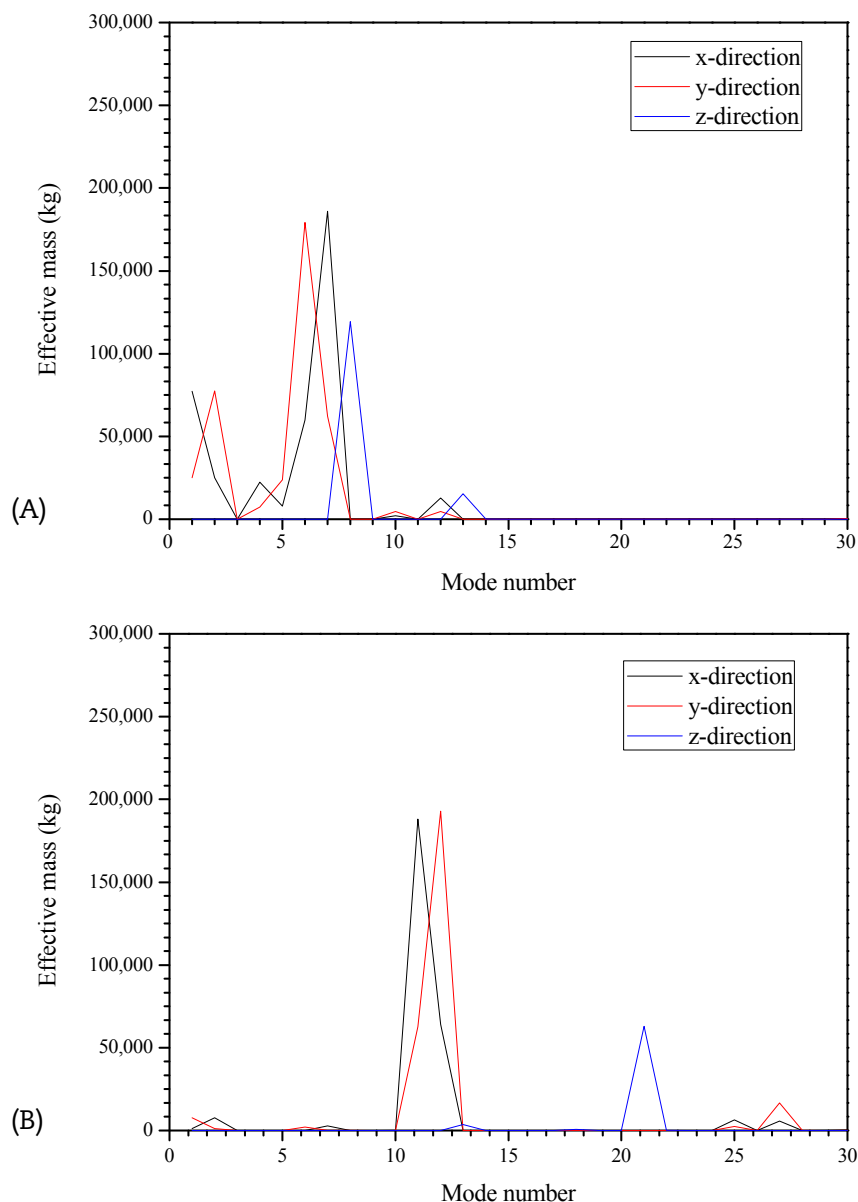
Fig. 12. Variation of effective masses. (A) Added-mass (A-M) model. (B) Fluid-structure (F-S) model.

Conflicts of interest

All authors have no conflicts of interest to declare.

References

[1] M.J. Jhung, Y.H. Ryu, Study on dynamic response of mechanical component to earthquake, J. Nucl. Sci. Technol. 47 (2010) 1065–1074.

[2] J.B. Park, Y.C. Choi, S.J. Lee, N.C. Park, K.S. Park, Y.P. Park, C.I. Park, Modal characteristic analysis of the APR 1400 nuclear reactor internals for seismic analysis, Nucl. Eng. Technol. 46 (2014) 689–698.

[3] J.F. Sigrist, D. Broc, C. Laine, Dynamic analysis of a nuclear reactor with fluid-structure interaction Part I: seismic loading, fluid added mass and added stiffness effects, Nucl. Eng. Des. 236 (2006) 2431–2443.

[4] Y.C. Choi, S.H. Lim, B.H. Ko, K.S. Park, Y.P. Park, K.H. Jeong, J.S. Park, Dynamic characteristics identification of reactor internals in SMART considering fluid-structure interaction, Nucl. Eng. Des. 255 (2013) 202–211.

[5] M.J. Jhung, Y.B. Kim, A study on modal characteristics of flow skirt using effective Young's modulus, Nucl. Eng. Technol. 44 (2012) 501–506.

[6] M.J. Jhung, S.O. Yu, Y.T. Lim, Dynamic characteristics of a partially fluid-filled cylindrical shell, Nuclear Engineering and Technology 43 (2) (2011) 167–174.

[7] M.J. Jhung, K.H. Jeong, Free vibration analysis of perforated plate with square penetration pattern using equivalent material properties, Nucl. Eng. Technol. 47 (2015) 500–511.

[8] S.H. Lim, Y.C. Choi, K.R. Ha, K.S. Park, N.C. Park, Y.P. Park, K.H. Jeong, J.S. Park, Dynamic characteristics of a perforated cylindrical shell for flow distribution in SMART, Nucl. Eng. Des. 241 (2011) 4079–4088.

[9] S.U. Han, D.G. Ann, M.G. Lee, K.H. Lee, S.H. Han, Structural safety analysis based on seismic service conditions for butterfly valves in a nuclear power plant, Sci. World J. 2014 (2014) 1–9.

[10] M.J. Jhung, W.G. Hwang, Seismic response of reactor vessel internals for Korean standard nuclear power plant, Nucl. Eng. Des. 165 (1996) 57–66.

[11] C. De, Y.Z. Qiang, X. Yabo, S. Hong, Numerical study on seismic response of the reactor coolant pump in advanced passive pressurized water reactor, Nucl. Eng. Des. 278 (2014) 39–49.

[12] J.J. Bommer, M. Papaspiliou, W. Price, Earthquake response spectra for seismic design of nuclear power plants in the UK, Nucl. Eng. Des. 241 (2011) 968–977.

[13] D.Y. Ko, K.H. Kim, Structural analysis of CSB and LSS for APR1400 RVI CVAP, Nucl. Eng. Des. 261 (2013) 76–84.

[14] M.J. Jhung, Assessment of thermal fatigue in mixing tee by FSI analysis, Nucl. Eng. Technol. 45 (2013) 99–106.

[15] ASME Boiler & Pressure Vessel Code, Section III – Nuclear Power Plant Components; Division 1-Subsection NG, Core Support Structure, American Society of Mechanical Engineers, 2007.

[16] D.H. Kim, Y.S. Chang, M.J. Jhung, Numerical study on fluid flow by hydrodynamic loads in reactor internals, Struct. Eng. Mech. 51 (2014) 1005–1016.

[17] G.C. Everstine, A symmetric potential formulation for fluid-structure interaction, J. Sound Vib. 79 (1981) 157–160.

[18] P. Kohnke, Theory reference for the mechanical APDL and mechanical applications, ANSYS Inc. (2009).

[19] Y.G. Choi, J.B. Park, S.J. Lee, N.C. Park, Y.P. Park, J.S. Kim, W.J. Roh, Model reduction methods for cylindrical structures in reactor internals considering the fluid–structure interaction, J. Nucl. Sci. Technol. 53 (2016) 204–222.

[20] X. Zhou, R. Yu, L. Dong, The Complex-Complete-Quadratic-Combination (CCQC) method for seismic responses of Non-classically Damped Linear MDOF system, in: Proceedings of the 13th World Conference on Earthquake Engineering, Vancouver, Canada, 2004.

[21] U.S. Nuclear Regulatory Commission, Regulatory Guide 1.60, Design response spectra for seismic Design of Nuclear Power Plants, U.S. Nuclear Regulatory Commission Office of Nuclear Regulatory Research, Washington D.C, 2014.

[22] U.S. Nuclear Regulatory Commission, Regulatory Guide 1.61, Damping Values for seismic Design of Nuclear Power Plants, U.S. Nuclear Regulatory Commission Office of Nuclear Regulatory Research, Washington D.C, 2007.